Supplementary Material for

Dynamic manipulation of mid-infrared polarized thermal emission enabled by In_3SbTe_2 metasurface

Guoqing Xu[a], Xizheng Zhang[b], Wei Wang[c], Mohammad Reza Zarei[a], Kai Guo[a], Qianlong Kang[a], Zhongyi Guo[a,*]

[a]*Hefei University of Technology, School of Computer and Information, Hefei, 230009, China*

[b]*Hefei University of Technology, School of Materials Science and Engineering, Hefei, 230009, China.*

[c]*Shijiazhuang Tiedao University, Department of Mathematics and Physics, Shijiazhuang 050043, China*

**guozhongyi@hfut.edu.cn.*

Supplementary Note 1: Refractive index of several phase change materials

Figure S1 presents the refractive indices of In_3SbTe_2 (IST) [45], $Ge_2Sb_2Te_4$ (GST224) [57], $Ge_2Sb_2Te_5$ (GST225) [58], and VO_2 [59] in both amorphous and crystalline states. Upon crystallization, IST transitions from a dielectric material to a metallic material. Amorphous IST is a semiconductor with atoms connected by covalent bonds, while crystalline IST is a "bad metal," where atoms are connected by metavalent bonds, resulting in higher conductivity. Figure S1 compares the refractive indices of IST with other common phase change materials like GST224, GST225, and VO_2. In the amorphous state, all phase change materials are almost lossless, with the imaginary part of the refractive index close to zero. However, in the crystalline state, IST not only exhibits the largest increase in refractive index but also possesses metallic-like characteristics (n < k).

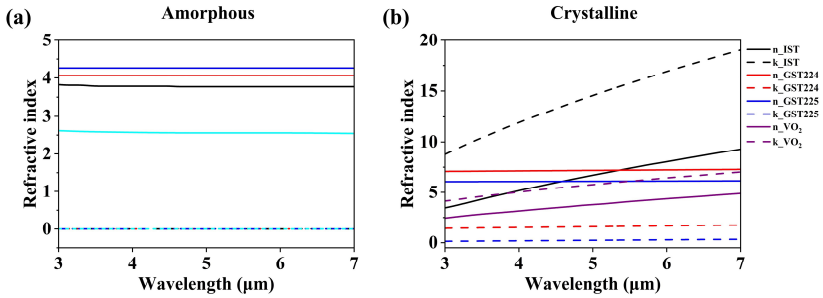

Figure S1. The refractive indices of IST and other common phase change materials in the (a) amorphous and (b) crystalline states.

Supplementary Note 2: Comparative analysis of different phase change materials

To demonstrate the advantages of the phase-change material IST used in this paper, VO_2 and GST225 (referred to as VO_2-CPME and GST-CPME, respectively) were used to replace IST in CPME. The structural parameters used in the simulations are the same as those in Figure 1. Figure S2 shows the spectral emissivity based on crystalline VO_2 and GST225. As shown in Figure S2(a), the spectral emissivity tuning range of VO_2-CPME is relatively small, whether for linear or circular polarization. For example, the emissivity of LCP and RCP differs by only about 0.1. This is because the metallicity of crystalline VO_2 is less than that of IST, resulting in a weaker chirality of the metal antenna. As shown in Figure S2(b), when GST is used instead of IST, the spectral emissivities of various polarization states in GST-CPME are nearly identical and at a lower level. From Figure S1, it can be seen that the metallicity of the phase-change material GST in its crystalline state is very weak, which results in weak chirality when GST is used as a metal antenna, and it is difficult to form plasmonic resonance.

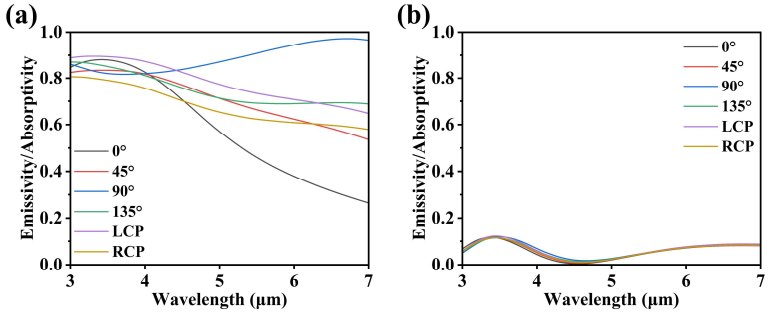

Figure S2. Spectral emissivity of (a) VO_2-CPME and (b) GST-CPME at different polarization angles.

Supplementary Note 3: Normalized electric field distribution of chiral metasurface when IST is in amorphous state

Figure S3 shows the normalized electric field distribution on the chiral metasurface under different polarized light incidences when IST is in amorphous state. Similarly, the wavelength of the incident light is 4.7μm. As shown in Figures S3(a)-(f), the electric field around the L-shaped and I-shaped antennas is relatively weak when different polarized light is incident on the metasurface. In the amorphous state, IST behaves as a dielectric, leading to a weak response to the incident light. Additionally, the presence of the bottom reflective layer causes most of the incident light to be reflected. Therefore, the CPME exhibits

consistent and low absorption for various polarized lights.

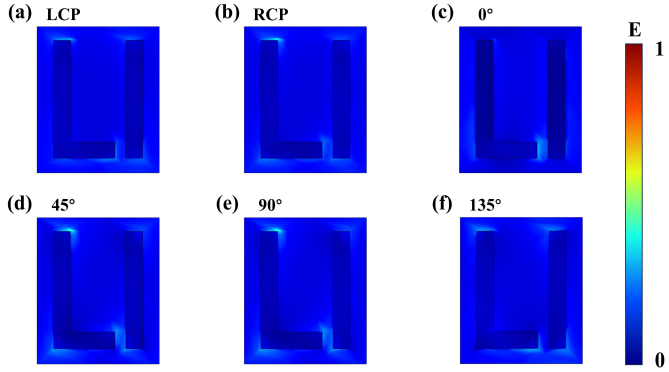

Figure S3. Normalized electric field distribution of the chiral metasurface with amorphous IST when (a) LC, (b) RC, (c) 0°, (d) 45°, (e) 90°, and (f) 135° polarized light is incident.

Supplementary Note 4: Normalized power loss distribution of chiral metasurface when IST is in amorphous state

Figure S4 shows the normalized power loss distribution on the chiral metasurface under different polarized light incidences when IST is in the amorphous state. The simulation depicts the power loss distribution at the resonant wavelength of 4.7μm. As shown in Figures S4(a)-(f), the power loss around the metal antennas is very weak when different polarized lights are incident on the metasurface. In the amorphous state, IST behaves as a dielectric, resulting in a weak response to the incident light. Furthermore, the presence of the bottom reflective layer causes most of the incident light to be reflected. Consequently, CPME exhibits uniformly low absorption characteristics for various polarized lights.

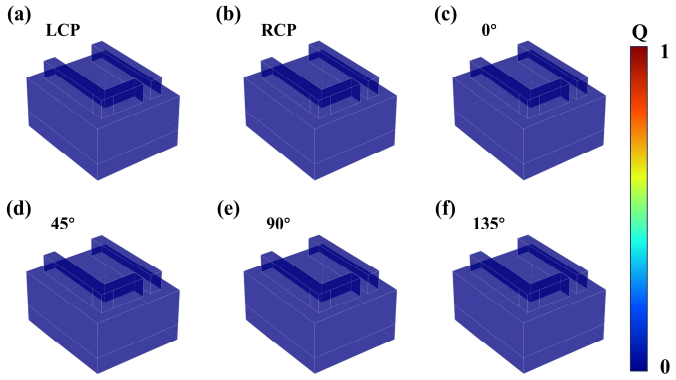

Figure S4. Normalized power loss distribution of the chiral metasurface with amorphous IST when (a) LC, (b) RC, (c) 0°, (d) 45°, (e) 90°, and (f) 135° polarized light is incident.

Supplementary Note 5: Effect of geometric perturbation segment l2 on DoCP of CPME

To control the intensity of the circularly polarized thermal emission of CPME, we introduced geometric perturbations that affect the symmetry of the unit cell. Below, we examine the effect of the geometric perturbation segment l2 on the DoCP of CPME in the MIR region, as shown in Figure S5. Except for the parameter l2, all other parameters are the same as those shown in Figure 1. According to equations (1) and (2) in the main text, the value of DoCP mainly depends on the LCP and RCP thermal emissions, so Figure S5 shows the emission spectra for LCP and RCP light. As shown in Figure S5(a), as the length of l2 increases from 0.15 μm to 0.55 μm, the LCP thermal emission steadily increases. As shown in Figure S5(b), the RCP thermal emission also increases with the length of l2, but the increase in RCP thermal emission is much smaller than that of LCP thermal emission. This is because, as l2 increases, the mirror symmetry and inversion symmetry of the unit cell are broken, forming a symmetry-broken structure, leading to the gradual emergence of spin-dependent thermal emission. Moreover, as l2 increases, spin-dependent thermal emission gradually strengthens. When l2 = 0.15μm, CPME has a geometrically symmetric structure, and the LCP and RCP thermal emissions are equal. When l2 = 0.55μm, the emission rate of CPME for LCP light reaches 0.86, while for RCP light, it only reaches 0.37. Figure S5(c)

calculates the DoCP of CPME for different sizes of l2, showing that as the length of l2 increases, the DoCP also increases. This indicates that the geometric perturbation segment plays a crucial role in spin-dependent thermal emission. The geometric perturbation segment l2 acts like a "knob," effectively and accurately controlling the intensity of circularly polarized thermal emission in the MIR range.

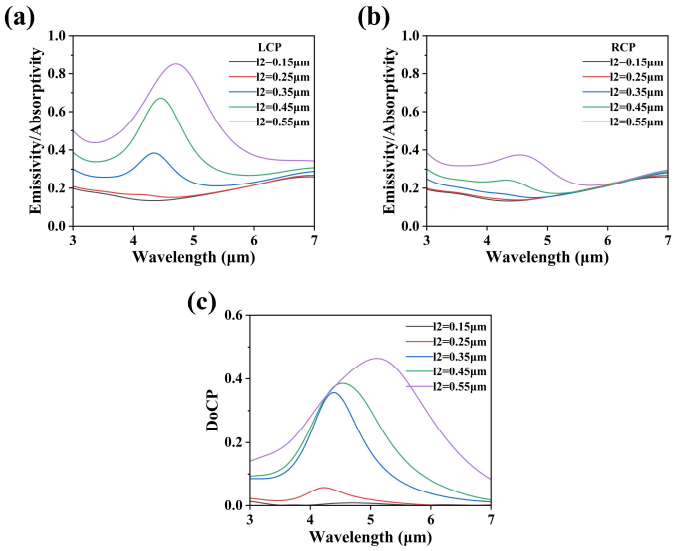

Figure S5. As l2 increases from 0.15μm to 0.55μm, (a) the LCP thermal emission spectra, (b) the RCP thermal emission spectra and (c) the DoCP of CPME.

Supplementary Note 6: Effect of thickness of dielectric layer on spectral emissivity of CPME

Finally, we discuss the effect of the dielectric layer (Al_2O_3) thickness on the spectral emissivity of CPME in the MIR region, as shown in Figure S6. All other parameters are the same as those shown in Figure 1, except for the thickness of the Al_2O_3 layer. As depicted in Figures S6 (a) and (e), as the thickness of the dielectric layer increases from 230nm to 630nm, the peak emissivity of 0° polarized light and LCP light first increases and then decreases, reaching the maximum when the thickness is 430nm. Figures S6 (b) and (c) show that as the thickness of the dielectric layer increases, the peak emissivity of 45° and 90° polarized light gradually decreases. Conversely, the peak emissivity of 135° polarized light and RCP light gradually increases with the increasing thickness of the dielectric layer, as shown in Figures S6 (d) and (f).

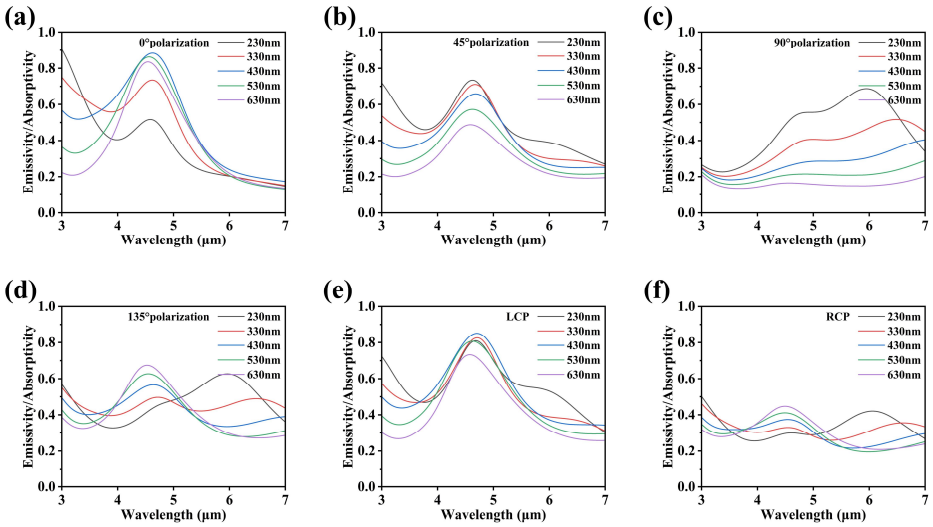

Figure S6. Simulated spectral emissivity/absorptivity of (a) 0°, (b) 45°, (c) 90°, (d) 135°, (e) LC, and (f) RC polarized light at different thicknesses of dielectric layer.